Journal of Hazardous Materials, 9 (1984) 139—157
Elsevier Science Publishers B.V., Amsterdam — Printed in The Netherlands

 1984

TRANSIENT CHARACTERISTICS OF DENSE GAS DISPERSION. PART I:

A DEPTH-AVERAGED NUMERICAL MODEL

ROBERT N. MERONEY

Fluid Mechanics and Wind Engineering Program, Department of Civil Engineering, Colorado State University, Fort Collins, CO 80523 (U.S.A.)

(Received September 29, 1983; accepted in revised form January 25, 1984)

Summary

A wind-tunnel validated, non-proprietary depth integrated numerical model is developed to calculate the behavior of heavy and cold gas clouds released into the atmosphere at ground level. The model (DENS20) is time dependent, quasi-three dimensional, and permits cloud heating from below and the entrainment of moist air. The model does not depend upon the Boussinesq assumption, but it does require the hydrostatic assumption. Model constants are set to fit a cross-section of data from wind-tunnel experiments on the transient and steady behavior of releases of heavy gases. Plume shape and concentration decay with distance and time are reproduced for comparative cases from the Porton Downs and China Lake field tests and the Colorado State University cold gas laboratory tests on dense gas behavior.

1.0 Introduction

A set of depth-integrated numerical models were developed to help interpret the behavior of heavy and cold gas experiments performed in meteorological wind tunnels. These models evolved from depth- or crosswind-averaged forms of the conservation equations of mass, momentum, species, and energy. Submodules permit alternate assumptions for the influence of wind profile, heat transfer, humidity, and air entrainment. The construction of these models reflects the philosophy of the model developed by Zeman [1]; however, since written computer listings are not available in the open literature for his or similar complexity models [2, 3], there are many differences in detail, and the numerical procedure used here is not similar at all.

A collection of papers which summarize field and laboratory measurements as well as the performance of several numerical models for dense gases was recently published by Britter and Griffiths [4]. In this collection Blackmore, Herman, and Woodward [5] review fifteen current mathematical models for the dispersion of accidental releases of heavy gases. The models are broadly classified into K-theory models (5 in number) and slab models

0304-3894/84/$03.00

(10 in number). The authors reviewed mechanistic features, applicability to differing types and geometries of release, and availability to users. An alternative, more detailed model typing scheme might consider five categories of increasing sophistication and plume physics:

(a) Modifications of classical Gaussian plume formulae developed for passive gases,
(b) Gravitational spread models which establish plume shape prior to a passive diffusion phase,
(c) Volume-integrated box models which asymptotically approach the passive diffusion phase,
(d) Depth- or cross-section averaged slab models, and
(e) Direct solution of the full three-dimensional conservation equations by finite difference or finite element approaches.

Category (b) include models which may or may not permit entrainment during the gravity spreading phase, but they transition to passive behavior abruptly once a specified criterion is exceeded. Categories (c) and (d) asymptotically approach passive plume behavior as gravity driving forces become insignificant. Categories (b), (c) and (d) are typed "slab" models by Blackmore et al. [5]. Category (e) models are generally most complex and flexible, but also require many ad hoc assumptions and the use of empirical expressions for eddy diffusivity (K-theory). Recently Chatwin [6] pointed out the limitations of deterministic models which solve only for mean concentrations. Meroney [7] extended the value of such calculations by using assumed probability distribution functions and empirical expressions for fluctuation moments to predict ignition regions for flammable gases. Most models are further distinguished from one another by the various ad hoc assumptions used for the mixing rates and the duration chosen for the gravity spread phase. Since various constants must be specified from experimental data, the results are often dependent on the data set used to calibrate the calculation scheme.

1.1 Depth-averaged models

A numerical model for dense cloud dispersion is desired which reproduces the detailed nuances of behavior perceived during laboratory and field experiments. Three-dimensional calculations are very expensive in computer storage and time. Fortunately, when the flow situation is only weakly three dimensional, so that one dimension can be decoupled from the other two, a set of relations obtained by integrating the conservation equations over that dimension realistically describes fluid motions. To be accurate the "depth-averaged" equations must have negligible vertical or lateral dynamic pressure gradients; hence, flow quantities are generally assumed to be constant or to have a similar distribution in the vertical and lateral directions.

Depth-averaged (advanced-slab, shallow-layer) models devised to describe heavy gas dispersal have been recommended by several investigators. Zeman [1] proposed such a model to describe the motion of buoyancy-conserved

releases of saline water from locks or the dispersion of gas plumes generated over pools of liquid natural gas (LNG). He developed expressions for transient two-dimensional or steady axisymmetric situations. The expressions he used did not consider heat transfer or humidity effects, and the numerical algorithms used were unstable.

Colenbrander [2] developed a steady-state model for the dispersion of dense gases by splicing together Gaussian plume profiles at the cloud edges and a well-mixed cloud core region so that the profiles become completely Gaussian far downwind. Plume growth is predicted by a set of semi-empirical equations for plume standard deviations in the lateral and vertical directions. A transient version of the model overcomes the limitations of being a steady-state model by means of repeated model runs using "observers" released to float over the cloud and report what they see. The model will not handle the zero wind speed case, does not consider heat transfer to the ground plane, and is proprietary.

Morgan, Morris, and Ermak [3] modified and extended Zeman's approach to include effects of turbulent mixing, atmospheric stability, height-dependent wind speed, source rate, and the flow of heat and momentum at cloud interfaces. The model does not appear to include the effects of atmospheric humidity. Their comprehensive model runs locally on a CDC 7600 computer via the Lawrence Livermore National Laboratory (LLNL) Octopus computer network. Unfortunately the code is rather cumbersome, the universal integrator subroutine used to solve the equations is rather slow, and the program is written in non-ASCII-standard LLNL Fortran.

Meroney and Lohmeyer [8] documented a computationally fast and numerically simple slab model which solves the depth-averaged mass continuity, momentum, and concentration equations for radially varying depth, and depth-averaged densities, velocities and concentrations. The model does not make the Boussinesq assumption, but it implicitly makes the hydrostatic pressure assumption (i.e., vertical velocities are assumed to be small). Model constants are tuned to fit a set of laboratory experiments on sudden releases of heavy gases. The model solves for the behavior of two-dimensional or radially symmetric advected clouds.

1.2 Criteria for present model

The depth-averaged model described below solves the layer-averaged lateral and longitudinal momentum, mass continuity, concentration and enthalpy equations for longitudinally varying depth and width and cross-section-averaged densities, temperatures, velocities, and concentrations. The model does not make the Boussinesq assumption; it permits surface heat transfer, humidity effects and water condensation, and velocity profile specification by friction velocity and surface roughness; it is computationally simple and fast; and the code is nonproprietary. Model constants are tuned to fit the laboratory data of Meroney and Lohmeyer [8] or Neff and Meroney [9]. The model is not as flexible or as universal as some of the models reviewed, but then it is also not as complex.

2.0 Formulation of the layer-averaged equations

The layer-averaged equations can be written for two-dimensional, radially symmetric, or laterally symmetric geometries. Two-dimensional and radially symmetric geometries are discussed by Meroney and Lohmeyer [8, 10]; hence, a laterally symmetric form of the equations will be provided here.

The formalism for creating layer-averaged conservation equations has been discussed in some detail by Ponce and Yabusaki [11]; hence, only a short review of the procedure will be provided here. The layer-averaged value of a mean variable Φ is defined as

$$\overline{\Phi} = \frac{1}{H} \int_0^H \int_0^B \Phi(x,y,z)\, dy dz \,. \tag{1}$$

Since mean variables are assumed distributed in a similar manner over the cross-section, covariances $\overline{\Phi_a \Phi_b}$ can be approximated as $\overline{\Phi_a \Phi_b} = \overline{\Phi}_a \cdot \overline{\Phi}_b$, and any residuals associated with this approximation are considered effective stresses and are included in diffusion terms. When entrainment takes place across the upper boundary of the cloud, H, then the upper boundary must obey

$$\frac{dH}{dt} + U_T \frac{dH}{dx} = W_T + w_e \,, \tag{2}$$

where U_T and W_T are the mean horizontal and vertical velocities at H, and w_e is the entrainment rate across the upper boundary. The mean hydrostatic pressure within the layer is found from

$$(p(x) - p_a(H)) = \frac{g}{H} \int_0^H \int_0^{z'} (\rho - \rho_a)\, dz' dz \,. \tag{3}$$

With the aid of the Leibnitz rule (see, e.g., Sokolnikoff and Redheffer [12]) the conservation equations can be integrated over the y–z plane cross-section areas. For a flow in which the x-axis is aligned with the wind vector the control volume is shown in Fig. 1. The final equations developed are nondimensionalized with respect to time, space, density, temperature, and energy scales equal to $T = H_0^{1/2}(g_0')^{-1/2}$, $L = H_0$, $r = \rho_a$, $\Delta T = T_a - T_0$, and $\Delta e = c_{p0}(T_a - T_0)$, respectively, where $g_0' = g((SG)_0 - 1)$. The final expressions used are the following.

Width equation

If the average width of the flow is $B(x)$, then by analogy to eqn. (2) we can define

$$\frac{dB}{dt} + U \frac{dB}{dx} = 2(V_g + v_e) \,. \tag{4}$$

Lateral momentum equation

The plume will spread laterally due to lateral hydrostatic forces which produce a lateral spread velocity, V_g. The lateral momentum will be retarded by surface drag; hence,

$$\frac{dM}{dt} + \frac{dUM}{dx} = \beta_1 \frac{(R-1)}{(R_0-1)} H^2 - \frac{C_f}{2} R V_g^2 (B_w - B_0)(HS) + \frac{1}{Re_T} \frac{d}{dx}\left(\frac{dM}{dx}\right) \quad (5)$$

where $M = RV_gHB$, twice the local half-section-averaged lateral momentum; (HS) = Heavyside operator (1 over source, 0 otherwise); $C_f/2$ = surface drag coefficient; β_1 = hydrostatic pressure constant; $1/Re_T$ = small numerical diffusivity to maintain stability; and $R = 1/\{(1-\theta T)\,[1-C+C\,(1-\beta)]\}$, an equation of state for local density in terms of mass fraction and temperature.

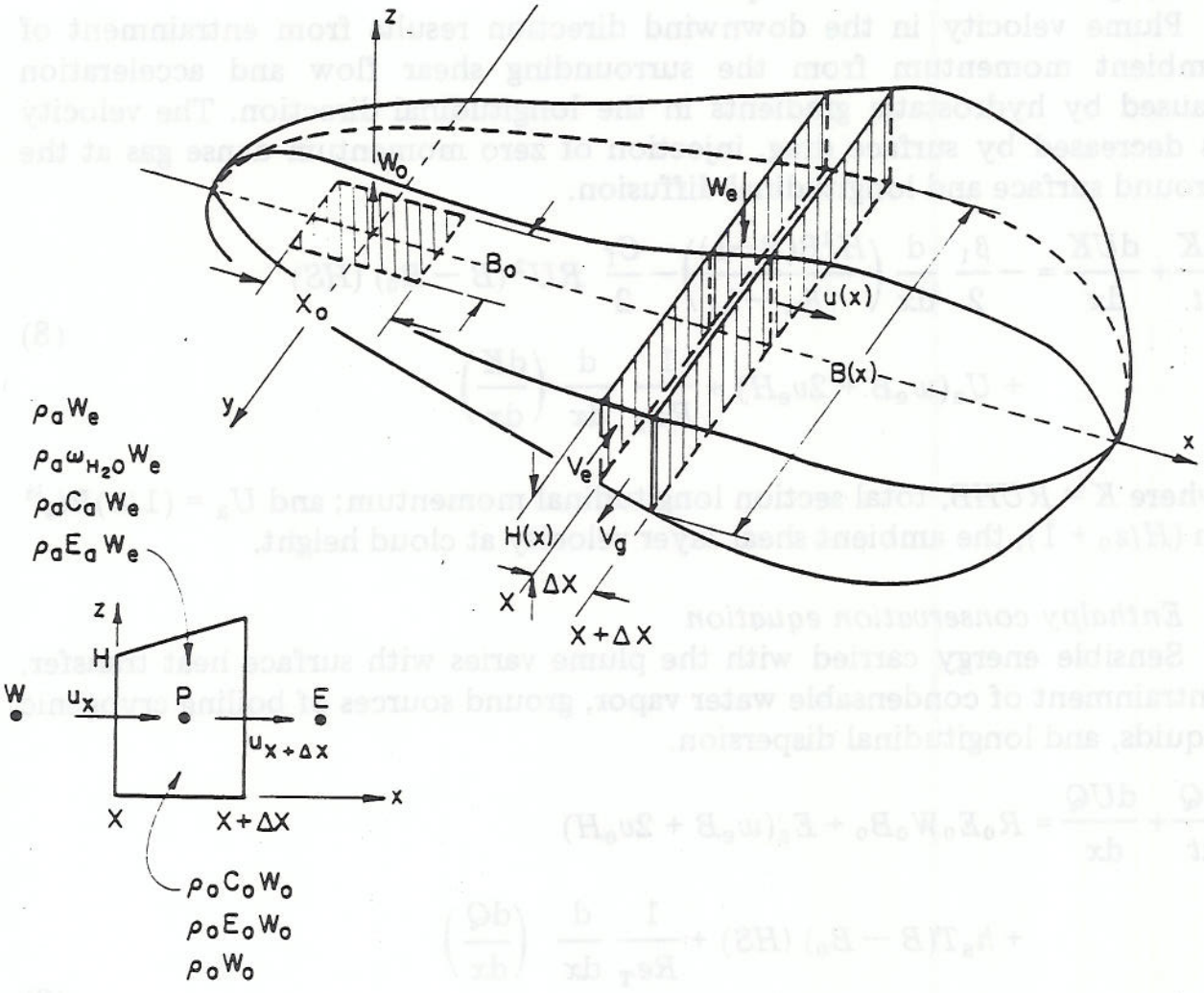

Fig. 1. Control volume for depth-averaged transport equations.

Mass conservation equation

Variation in the mass flux passing through any section is due to entrainment of ambient air across plume boundaries and ground level sources due to boiling of cryogenic pools.

$$\frac{dN}{dt} + \frac{dUN}{dx} = w_e B + 2v_e H + RW_0B_0 + \frac{1}{Re_T} \frac{d}{dx}\left(\frac{dN}{dx}\right) \quad (6)$$

where $N = RHB$, total section mass, and W_0, B_0 = source values of width and boiloff velocity.

Mass fraction conservation equation

The dense gas species is conserved as it advects from section to section. Boiloff from a surface pool of cryogenic liquid may add to the local flux values and longitudinal diffusion may decrease the values.

$$\frac{dP}{dt} + \frac{dUP}{dx} = R_0 W_0 B_0 + \frac{1}{Re_T}\frac{d}{dx}\left(\frac{dP}{dx}\right) \tag{7}$$

where $P = RCHB$, total section mass fraction; and R_0 = source value of density.

Longitudinal momentum equation

Plume velocity in the downwind direction results from entrainment of ambient momentum from the surrounding shear flow and acceleration caused by hydrostatic gradients in the longitudinal direction. The velocity is decreased by surface drag, injection of zero momentum dense gas at the ground surface and longitudinal diffusion.

$$\begin{aligned}\frac{dK}{dt} + \frac{dUK}{dx} = &-\frac{\beta_1}{2}\frac{d}{dx}\left(\frac{H^2B(R-1)}{(R_0-1)}\right) - \frac{C_f}{2}RU^2(B-B_0)(HS) \\ &+ U_a(w_eB + 2v_eH) + \frac{1}{Re_T}\frac{d}{dx}\left(\frac{dK}{dx}\right)\end{aligned} \tag{8}$$

where $K = RUHB$, total section longitudinal momentum; and $U_a = (1/k)Ri_*^{1/2}$ ln $(H/z_0 + 1)$, the ambient shear layer velocity at cloud height.

Enthalpy conservation equation

Sensible energy carried with the plume varies with surface heat transfer, entrainment of condensable water vapor, ground sources of boiling cryogenic liquids, and longitudinal dispersion.

$$\begin{aligned}\frac{dQ}{dt} + \frac{dUQ}{dx} = &R_0E_0W_0B_0 + E_a(w_eB + 2v_eH) \\ &+ h_sT(B-B_0)(HS) + \frac{1}{Re_T}\frac{d}{dx}\left(\frac{dQ}{dx}\right) \\ &+ (HS)(L_h)(\omega_{\Phi,T_a} - \omega_{100,T})(w_eB + 2v_eH - R_0W_0B_0) \\ &+ (HS)(L_h)RB(1-C)\omega_{100,T}\frac{4886}{T^2}(T_a - T_0)\frac{dT}{dx}\end{aligned} \tag{9}$$

where $Q = REHB$, total section enthalpy; $E = -(1+Cs_m)T^*/(1+s_m)$, the local section-averaged enthalpy; $\omega_{\Phi,T}$ = water vapor mass fraction at relative

humidity Φ, and temperature T; $L_h = (l_{H_2O})/(c_{p0}(T_a - T_0))$, the latent heat of vaporization of water; $h_s = 0.32\,[(Gr/Re^3Pr)Ri^*]^{1/2}[(1 + Cs_m)/(1 + s_m)]\,RT^{*1/2}$, the local surface heat transfer coefficient; $\beta = 1 - M_a/M_0$, a dimensionless source molecular weight; $\theta = 1 - T_0/T_a$, a dimensionless source temperature; $s_m = c_{p0}/c_{pa} - 1$, a dimensionless source specific heat capacity; and Gr, Re, Pr, Ri_* = Grashof, Reynolds, Prandtl and Richardson number scales, respectively, as defined in the list of symbols.

An equation of state which relates mass fraction, C, to molar or volume fraction, χ, is also useful:

$$\chi = C(1 - \beta)/[1 - C + C(1 - \beta)] \tag{10}$$

2.1 Water condensation and surface flux algorithm

The last two expressions in eqn. (9) adjust for heat initially released when the cold plume entrains water vapor, but which is subsequently re-evaporated when the temperature of the plume exceeds ambient dew point. The relations only condense water vapor which exceeds the local saturation values. In these two terms (HS) is the Heavyside operator which equals one when $T \leqslant T_{dewpoint}$ and zero otherwise. The dimensionless heat transfer coefficient, h_s, is based on the bulk transfer coefficient for mixed free and forced convection in the atmosphere recommended by Leovy [13]. Alternative values for fully forced or fully free convection can also be used.

2.2 Entrainment algorithms

Entrainment rates are perturbations on the forms suggested by Eidsvik [14] and Ermak et al. [15]. Some other forms tried are reviewed in Meroney and Lohmeyer [8]. The recommended entrainment expressions are:

$$w_e = c_z V_g + \frac{\alpha_4 v_*}{\alpha_4/\alpha_6 + Ri_*/RH^2} \tag{11}$$

$$v_e = \frac{3.24 H v_*}{B} \tag{12}$$

$$v_*^2 = \alpha_3^2/Ri_* + \alpha_2^2 \left[\frac{Gr(1 + s_m)(1 - \theta T^*)}{Re^2 (1 + Cs_m)(1 - \theta)} Hh_s T^* \right]^{2/3} \tag{13}$$

These relations retain a near source term which produces entrainment due to gravity spreading in a calm environment. Expressions by Zeman [1] and Morgan et al. [3] also allow for such a condition. A major difference here is all unspecified constants are determined by comparison to the laboratory data of Meroney and Lohmeyer [8, 10, 16] and Neff and Meroney [9], but once the values were chosen they were not varied during the validation exercises discussed in Section 4.0.

3.0 Numerical method (DENS20)

Equations (4)–(9) were developed in a difference form using an implicit, second-upwind-difference, donor-cell approach. The difference equations were solved by the Thomas or tri-diagonal algorithm. Step sizes in time were limited to

$$\Delta t < \frac{0.25\,\Delta x}{u_{max} + c_{max}}$$

where c_{max} is the maximum local wave speed, and the wave speed is defined as $c = (g'H)^{1/2}$. The algorithms maintained accurate conservation of the original cloud mass. The calculations lost less than 0.5% of the mass over the integration periods studied. Raithby [17] suggests that upwind-difference schemes introduce damping due to transient behavior as well as spatial variations. Alternative schemes were examined, such as the flux-corrected-transport scheme of Book et al. [18] and the smoothing algorithm of P.E. Long, however, the extra complication resulted in only small variation in the results.

Constants found to fit the wind-tunnel data most satisfactorily are c_z = 0.05, α_2 = 0.5, α_3 = 1.0, α_4 = 2.0, α_6 = 0.3, β_1 = 0.153, $C_f/2$ = 0.0025 and $1/Re_T$ = 0.0.

4.0 Validation examples

The credibility of a numerical model depends upon its ability to reproduce accurately the values of plume size and concentration distribution found during field experiments. The field data selected for comparison to the DENS20 program include instantaneous releases of isothermal dense gases, liquid natural gas (LNG) spills on water, and continuous releases of cold dense gases in a wind tunnel.

4.1 DENS20 model comparisons with Porton Downs field experiment

The Porton Downs field trials used a gas source in the form of a cubical box of about 3.5 m per side containing 40 m^3 of gas. The gas was released by allowing the sides of the box (made of thin pleated tarpaulin material) to collapse to the ground under gravitational forces in about 0.8 seconds, leaving a cube of the dense gas suddenly exposed to the prevailing wind conditions [19]. A total of 42 individual trials were run, covering a wide range of wind speeds, released gas density, surface roughness, atmospheric stability and ground slope. Measurements included visual records of plume outline as evidenced by tracer smoke and dosage and continuous concentration monitors. The gases released were mixtures of freon (CCl_2F_2) and air adjusted to specific gravities ranging from 1.2 to 4.2.

Hall, Hollis and Ishaq [20] reproduced the behavior of Runs 3, 8, 21, 29, 33, and 37 from the Porton trials in a set of wind-tunnel experiments. In

all cases they reproduced the time variation of plume width, plume shape, plume arrival and plume departure very well. There were very strong similarities between the visual appearance of the field and model plumes. Comparisons were also made between field concentration measurements and the model measurements. Some of the comparisons showed very good agreement, but others were poor. Differences were attributed to the naturally occurring high levels of repeat variability and anomalies in the field measurements. (In some cases the data from integrated continuous monitors and dosage monitors placed side by side varied by more than an order of magnitude.)

These same situations were calculated by the slab model. In each case the model replicated the Hall et al. behavior quite well and differed from the field data in the same manner that their tests did. Porton trial number 8 results are shown in Figs. 2, 3, and 4. The field test was performed at wind speeds below the threshold values of the instruments available; hence, the trial experiment was effectively in still air. Figure 2 displays peak concentrations measured at different downwind locations. The Hall et al. model test, the slab model and a box model [16] agree very well, but the field

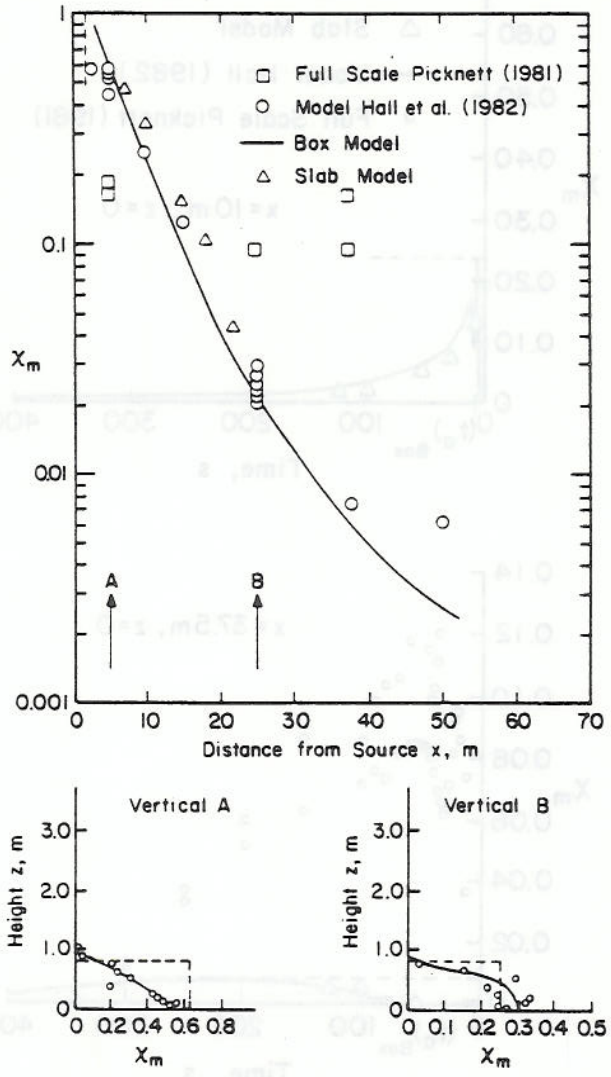

Fig. 2. Porton trial no. 8 — Peak concentrations in cloud.

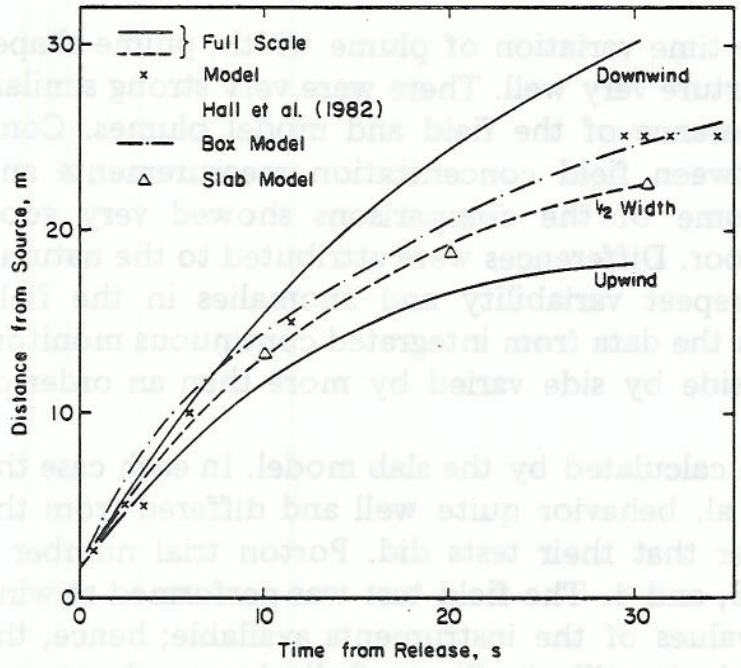

Fig. 3. Porton trial no. 8 — Cloud size variation.

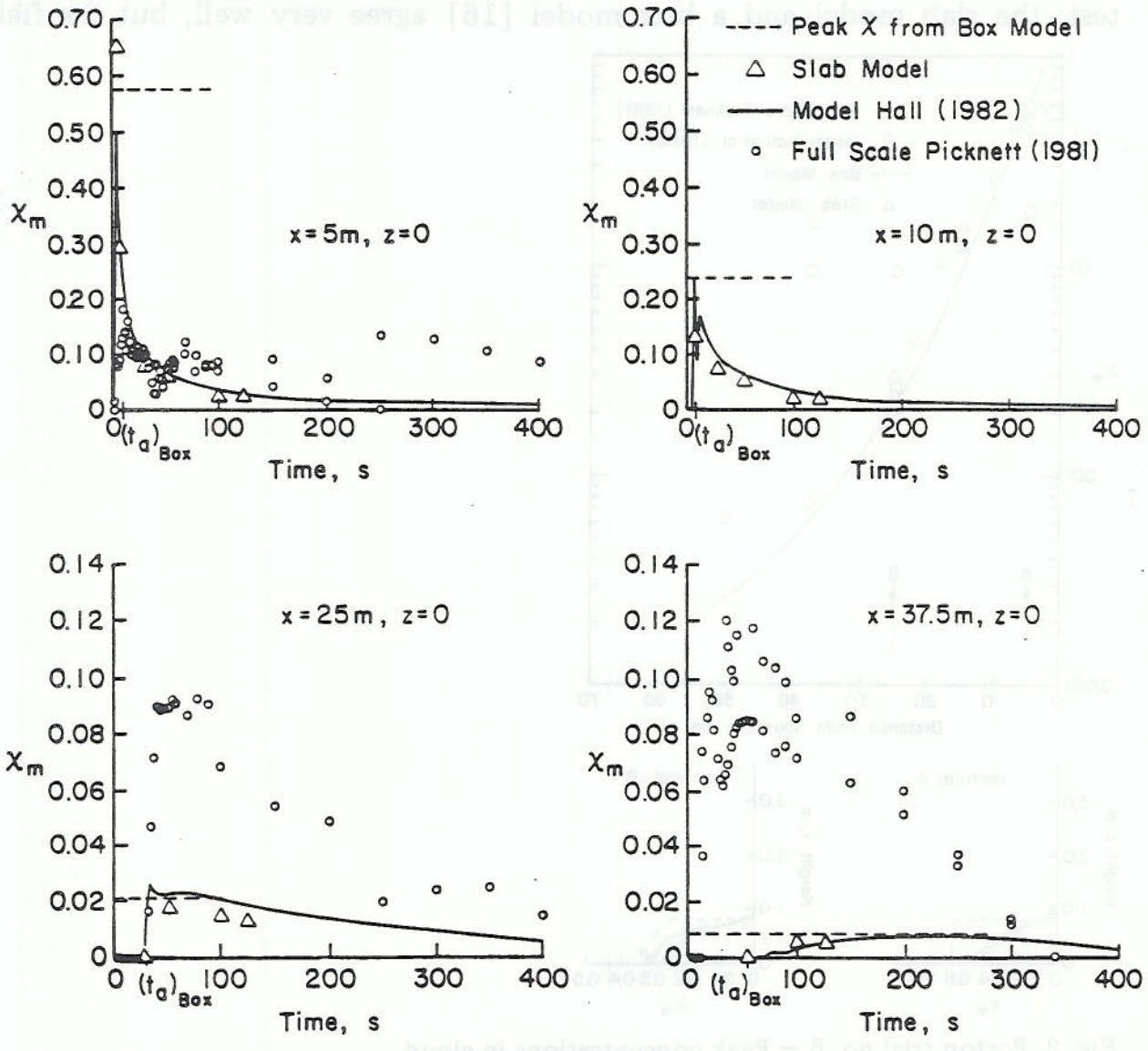

Fig. 4. Porton trial no. 8 — Continuous monitor measurements.

measurements do not seem to vary at all with distance. Figure 3 compares wind-tunnel, full-scale, slab model, and box model cloud widths at various times from release. Agreement is excellent. Figure 4 displays concentration versus time traces at various radial locations. The slab model predicts the Hall et al. wind-tunnel simulation of peak concentration, arrival time, and arrival of the maximum concentration very well. The larger concentrations and early arrival times found during the field test suggest that locally the wind was gusting and the average wind speed was not effectively zero.

4.2 DENS20 comparisons with China Lake field experiments

Puttock, Blackmore, and Colenbrander [21] conclude in their evaluation of field experiments that only Test 8 of the Burro experiments was strongly influenced by density effects. Since diffusion during the other tests resembled conventional passive dispersion behavior a comparison with their data are not as interesting (both slab and box models predicted concentration decay very well). During the Burro 8 Field Trial at China Lake Naval Weapons Center 28.4 m^3 of LNG was released at a rate of 16.0 m^3/min onto a small water pond. The wind speed was 1.8 ± 0.3 m/s and decreasing at a 1 m height, while the atmospheric stability was slightly stable. Humidity was measured to be 5% upwind of the spill and air temperature was 33°C. Since the plume mixed violently over the pond due to rapid boiling it is likely that humidity downwind of the pond is higher (say 20%). This spill displayed the most gravity-dominated behavior of those performed. (See Koopman et al. [22] and Meroney and Neff [23] for a discussion of field data.)

The slab model described in Sections 2.0 and 3.0 was run for Burro 8 initial conditions for (a) adiabatic entrainment of dry air and (b) mixed convection heat transfer and entrainment of air at 20% humidity. The maximum concentrations of methane, C_m, versus downwind distance, x, are plotted in Fig. 5. Both predictions are well within the scatter of the field data. Water vapor condensation and heat transfer initially result in somewhat accelerated dilution out to 150 m; however, subsequent re-evaporation of condensed water vapor re-cools the plume and the two curves rejoin one another. Although the effect of heat transfer and the humidity are to accelerate entrainment, they also reduce the plume lateral spread significantly as shown in Fig. 6. This reduction of plume surface area seems to compensate for any increased entrainment rate; hence, plume concentrations are only slightly modified by heat transport along the center line of advection. Since the wind speeds involved in Burro 8 are quite small and the boiloff times short, calculations were performed assuming that the entire volume was released instantaneously, and then they were repeated with the boiloff spread over the observed release time. Plots of the transient behavior of the LFL mean concentration of 5% are displayed in Figs. 7 and 8.

A cross-section of plume concentration at x = 140 m at a time after release of 200 s is shown in Fig. 9. These isopleths were created from the

predicted slab data for plume height, width, and centerline concentration by distributing the plume in the manner suggested by Ermak et al. [15] where $C_m(x,y,z) = C_m(x,0,0)\ [1-(2y/3B)^2] \cdot [1-(2z/3H)^2]$. Measured isopleths are plotted in the same figure for comparison. The slab model could not reproduce the lateral variations in plume height and circulation associated with cloud side wall gravity head, horseshoe vortices, and local terrain. To reproduce these details a category (e) type three-dimensional model is required.

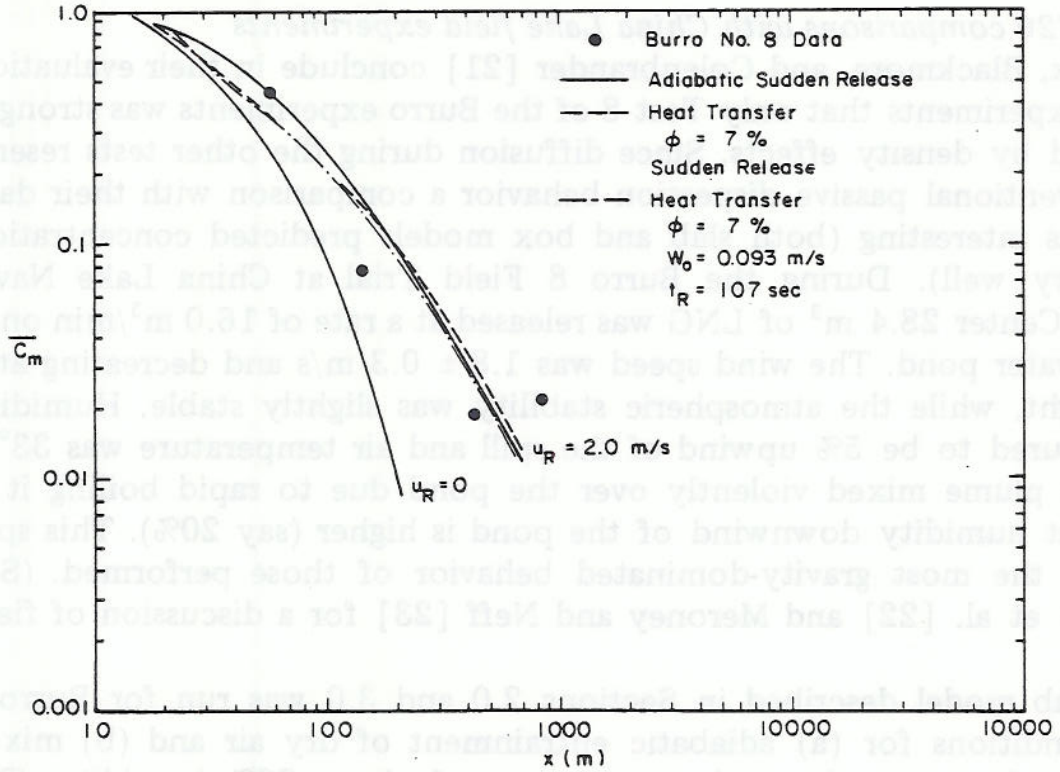

Fig. 5. Burro trial no. 8 — Peak concentrations at ground level.

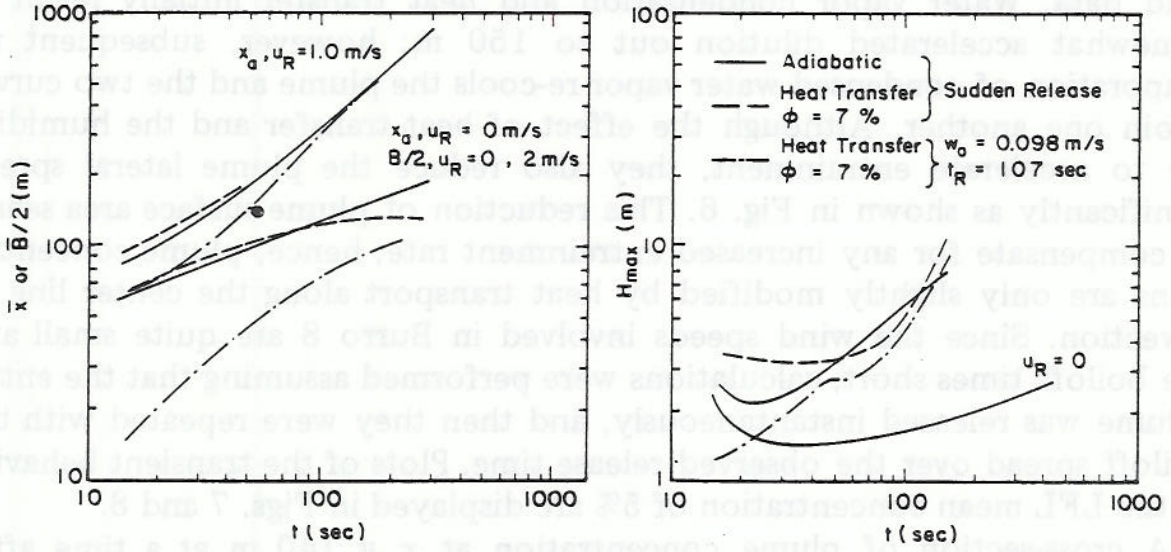

Fig. 6. Burro trial no. 8 — Cloud size variation.

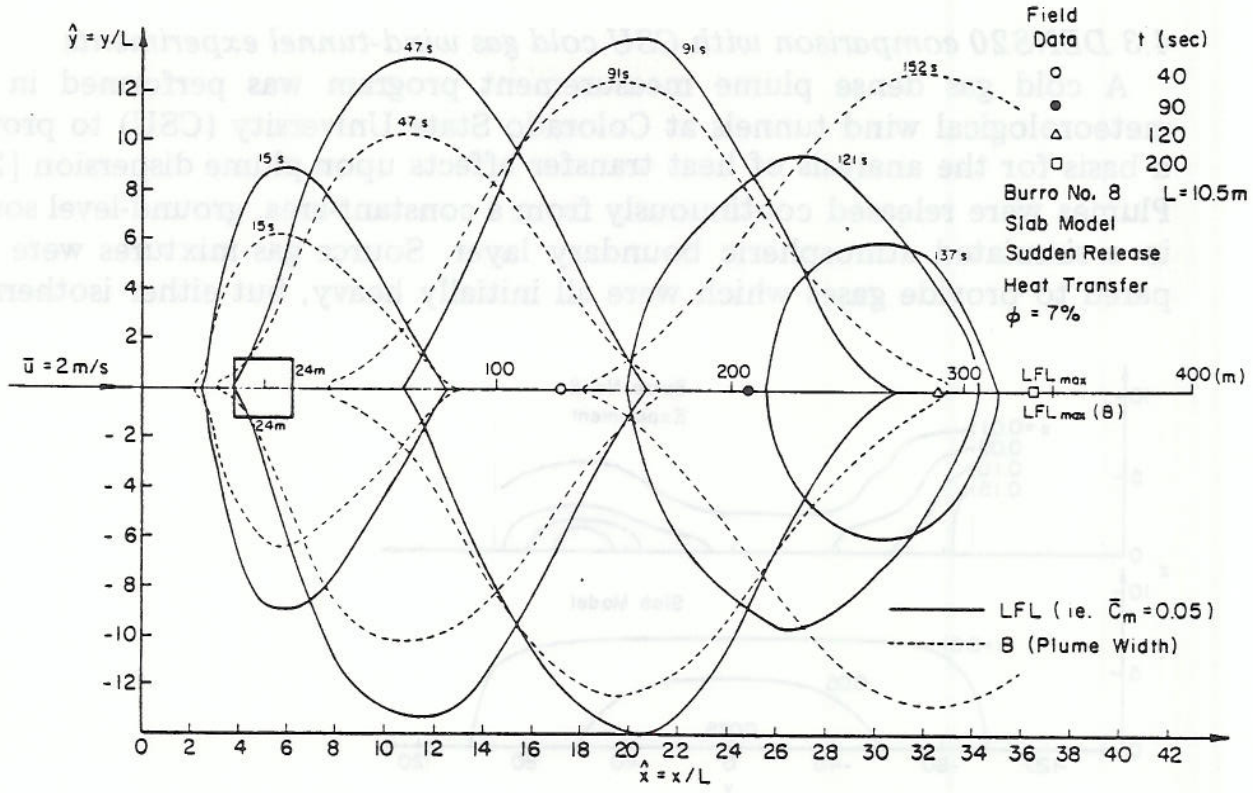

Fig. 7. Burro trial no. 8 — Transient behavior of the LFL mean concentration of 5%, sudden cloud release.

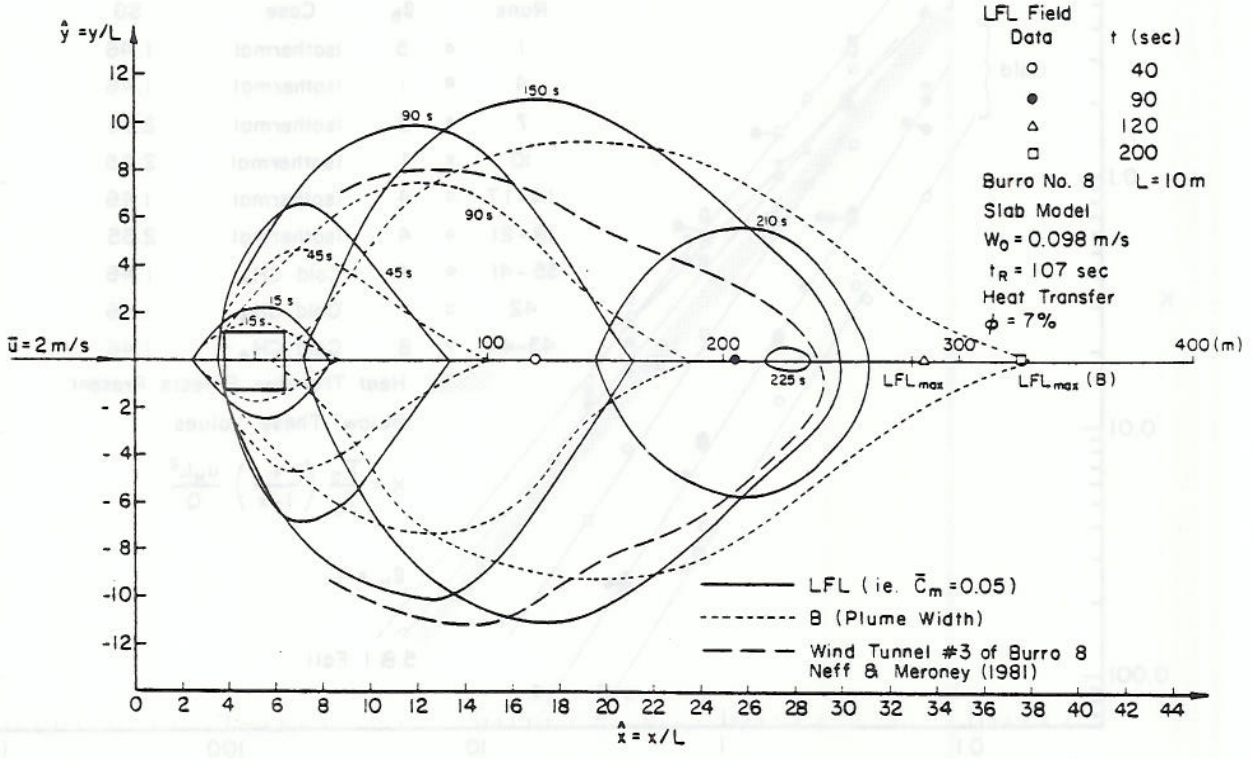

Fig. 8. Burro trial no. 8 — Transient behavior of the LFL mean concentration of 5%, finite boiloff time.

4.3 DENS20 comparison with CSU cold gas wind-tunnel experiments

A cold gas dense plume measurement program was performed in the meteorological wind tunnels at Colorado State University (CSU) to provide a basis for the analysis of heat transfer effects upon plume dispersion [24]. Plumes were released continuously from a constant-area, ground-level source in a simulated atmospheric boundary layer. Source gas mixtures were prepared to provide gases which were all initially heavy, but either isothermal,

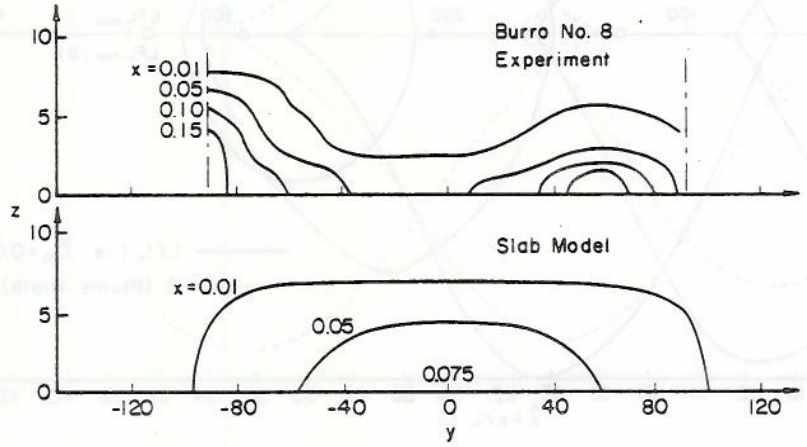

Fig. 9. Burro trial no. 8 — Concentration cross-section at 140 m at 200 s.

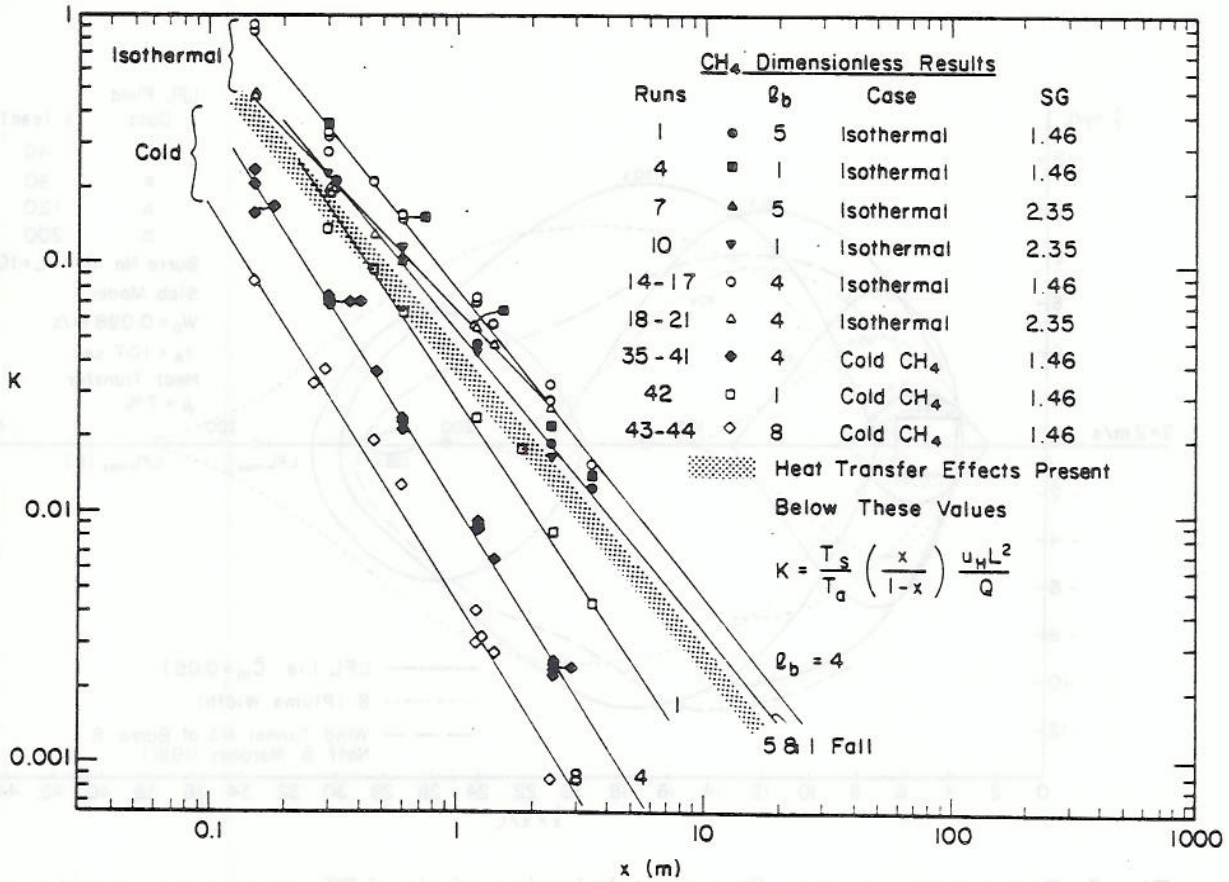

Fig. 10. CSU wind-tunnel tests — Cold dense gas concentration coefficient, K, versus down-wind distance — Data.

cold with source specific heat capacity equal to that of air, or cold with source specific heat capacity greater than that of air. Thus one could evaluate whether dilution resulted from adiabatic entrainment mechanisms, heat transfer effects, or unbalanced thermal expansion. Two buoyancy

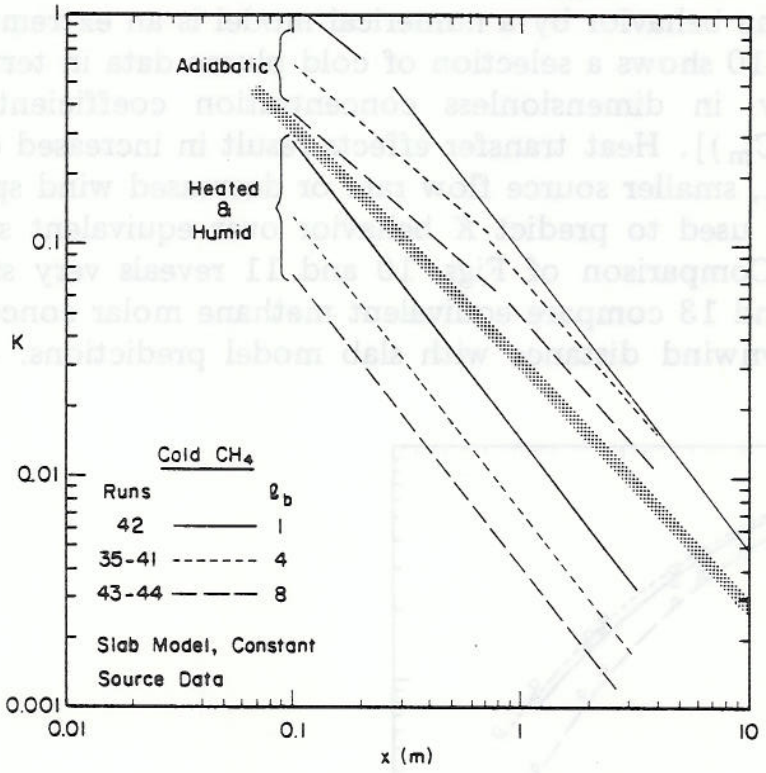

Fig. 11. CSU wind-tunnel tests — Cold dense gas concentration coefficient, K, versus down-wind distance — Numerical prediction.

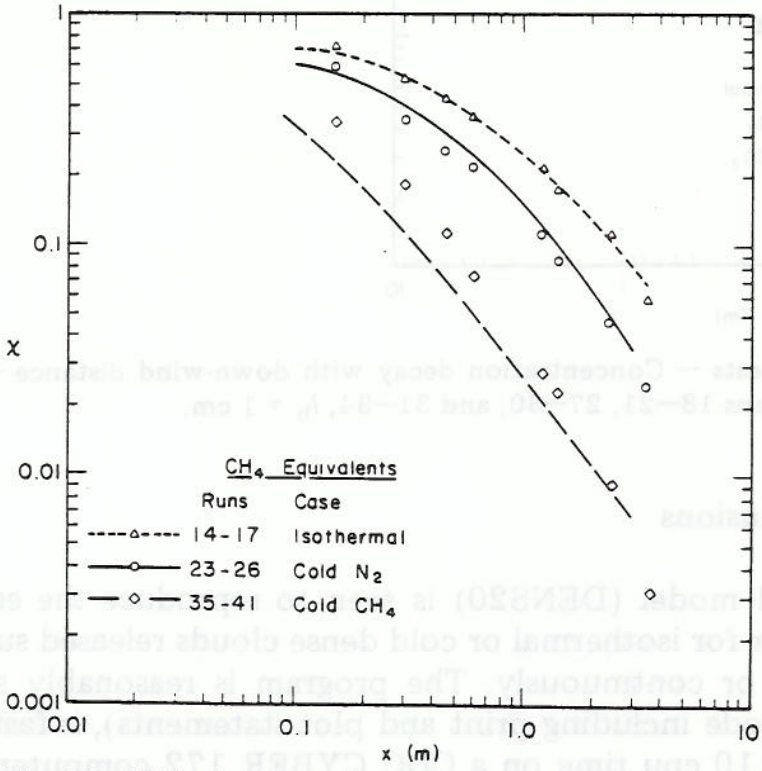

Fig. 12. CSU wind-tunnel tests — Concentration decay with down-wind distance — Data and numerical prediction, runs 14—17, 23—26, and 35—41, l_b = 4 cm.

conditions were examined such that the buoyancy length scale, l_b, varied from 1.0 to 8.0 cm, but the source conditions were selected to maintain flux Froude number equality among cases. Gases released included CCl_2F_2–air mixtures, cold nitrogen, cold carbon dioxide, and cold methane.

Tests at laboratory scales exaggerate heat transfer effects; therefore, duplication of the plume behavior by a numerical model is an extreme test for any model. Figure 10 shows a selection of cold plume data in terms of the along-wind decay in dimensionless concentration coefficient, $K = C_m U_R H_0^2 T_a / [T_0 Q(1-C_m)]$. Heat transfer effects result in increased decay rate as l_b increases (i.e., smaller source flow rate or decreased wind speed).

The slab model was used to predict K behavior over equivalent source and flow conditions. Comparison of Figs. 10 and 11 reveals very similar behavior. Figures 12 and 13 compare equivalent methane molar concentration decay versus downwind distance with slab model predictions. Again agreement is excellent.

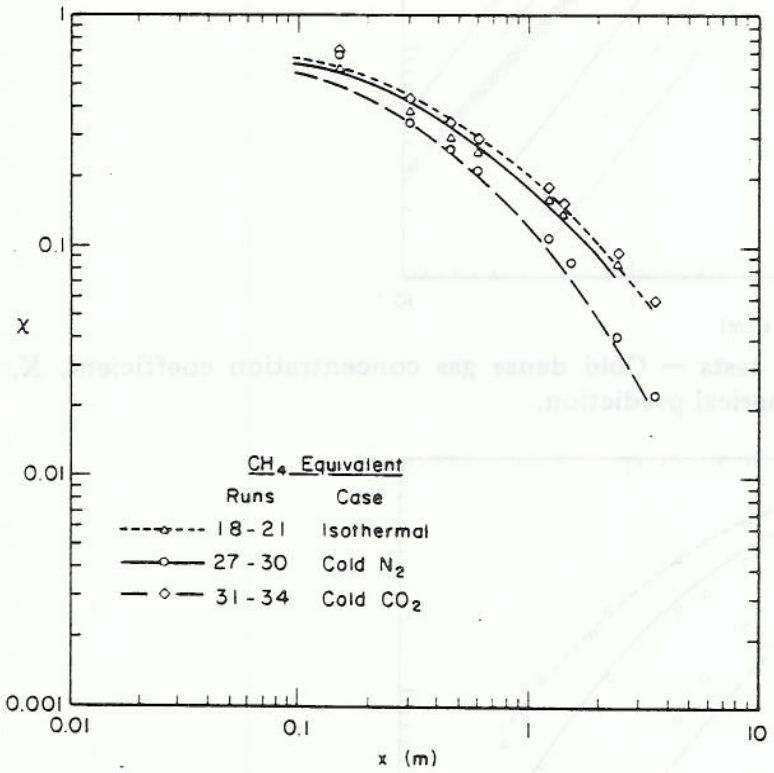

Fig. 13. CSU wind-tunnel tests — Concentration decay with down-wind distance — Data and numerical prediction, runs 18—21, 27—30, and 31—34, l_b = 1 cm.

5.0 Summary and conclusions

The depth-integrated model (DENS20) is seen to reproduce the essence of dense cloud behavior for isothermal or cold dense clouds released suddenly, over a finite time, or continuously. The program is reasonably simple (350 lines of Fortran code including print and plot statements), is fast (320 time steps forward in 110 cpu time on a CDC CYBER 172 computer), and

does not occupy a large amount of computer memory (a version of the program written in BASIC occupies less than 64 k on an IBM PC microcomputer).

This model-building exercise has shown that reasonably accurate but inexpensive programs can be produced for hazard analysis. Systematic calculations with this physically realistic model provide an opportunity to examine transient plume characteristics often seen in the field but difficult to measure accurately. The companion Part II paper which follows examines a number of interesting dense gas cloud characteristics.

Acknowledgements

The author wishes to acknowledge support from the Institute Wasserbau III, University of Karlsruhe, F.R.G.; the von Humboldt Foundation, F.R.G.; and the Gas Research Institute, U.S.A.

List of symbols

B	Plume width
C	Concentration mass fraction
$C_f/2$	Surface drag coefficient
c_p	Specific heat capacity
E	Enthalpy
g'	Gravitational constant
Gr	Grashof number, $g\beta(T_a - T_0)H_0/\nu_a^2$
H	Plume height
(HS)	Heavyside operator
h_s	Surface heat transfer coefficient
k	Von Karman constant
K	See eqn. (8), section longitudinal momentum
l_b	Buoyancy length scale
L_h, l_{H_2O}	See eqn. (9), latent heat of vaporization of water vapor
M	See eqn. (5), section lateral momentum, or molecular weight
N	See eqn. (6), section mass
p	Pressure
P	See eqn. (7), section mass fraction
Pr	Prandtl number
Q	See eqn. (9), section enthalpy, or plume source strength
R	See eqn. (5), plume density
Re	Reynolds number, $(g'_0 H)^{1/2} H/\nu_a$
Ri_*	Richardson number, $(g'_0 H_0)/u_*^2$
(SG)	Specific gravity
t	Time
T	Temperature, or time scale
T^*	Dimensionless temperature, $(T - T_0)/(T_a - T_0)$
u, U	Velocity, velocity scale

u_*	Friction velocity
U_T, W_T	Advection velocities at cloud top
v_e, w_e	Entrainment velocities
V_g	Gravity spread velocity
χ	Mole fraction concentration
x,y,z	Coordinates
z_0	Surface roughness
ν	Kinematic viscosity
ρ	Density
α, β, Re_T	Constants

Subscripts

a	Ambient air conditions
m	Maximum
0	Initial value or ground level
R	Reference value

Superscripts

	Ensemble average

References

1 O. Zeman, The dynamics and modeling of heavier-than-air, cold gas releases, Atmos. Environ., 16(4) (1982) 741—751.

2 G.W. Colenbrander, A mathematical model for the transient behaviour of dense vapour clouds, 3rd International Symposium on Loss Prevention and Safety Promotion in the Process Industries, Basel, Switzerland, 1980, 29 pp.

3 D.L. Morgan, Jr., L.K. Morris and D.L. Ermak, SLAB: A time-dependent computer model for the dispersion of heavy gases released in the atmosphere, Lawrence Livermore National Laboratory, Livermore, California, Report UCRL-53383, 1983, 15 pp.

4 R.E. Britter and R.F. Griffiths (Eds.), Dense Gas Dispersion, Elsevier Scientific Publishing Company, Amsterdam, 1982.

5 D.R. Blackmore, M.N. Herman and J.L. Woodward, Heavy gas dispersion models, J. Hazardous Materials, 6 (1982) 107—128.

6 P.C. Chatwin, The use of statistics in describing and predicting the effects of dispersing gas clouds, J. Hazardous Materials, 6 (1982) 213—230.

7 R.N. Meroney, Unsteady behavior of a simulated LNG vapor cloud suddenly released into a wind-tunnel boundary layer, Proceedings of American Gas Association Transmission Conference, May 2—4, 1983, Seattle, Washington, AGA, Arlington, VA, 1983, 21 pp.

8 R.N. Meroney and A. Lohmeyer, Gravity spreading and dispersion of dense gas clouds released suddenly into a turbulent boundary layer, Gas Research Institute Report GRI 81/0025, Chicago, Illinois, U.S.A., 1982, 220 pp.

9 D.E. Neff and R.N. Meroney, The behavior of LNG vapor clouds: Wind-tunnel tests on the modeling of heavy plume dispersion, Gas Research Institute Report GRI 80/0145, Chicago, Illinois, U.S.A., 1982, 120 pp. (Data Appendix is GRI 80/0145.1, 161 pp.)

10 R.N. Meroney and A. Lohmeyer, Statistical characteristics of instantaneous dense gas clouds released in an atmospheric boundary layer wind tunnel, J. Boundary-Layer Meteorol., Vol. 28, 1984, 38 pp.

11 V.M. Ponce and S.B. Yabusaki, Mathematical modeling of circulation in two-dimensional plane flow. National Science Foundation Final Report, Grant No. CME 7805458, 1980, 131 pp.
12 I.S. Sokolnikoff and R.M. Redheffer, Mathematics of Physics and Modern Engineering, McGraw Hill, New York, 1958, 812 pp.
13 C.B. Leovy, Bulk transfer coefficient for heat transfer, J. Geophys. Res., 74(13) (1969) 3313—3321.
14 K.J. Eidsvik, A Model for heavy gas dispersion in the atmosphere, Atmos. Environ., 14 (1980) 769—777.
15 D.L. Ermak, S.T. Chan, D.L. Morgan and L.K. Morris, A comparison of dense gas dispersion model simulations with Burro series LNG spill test results, J. Hazardous Materials, 6 (1982) 129—160.
16 R.N. Meroney and A. Lohmeyer, Prediction of propane cloud dispersion by a wind-tunnel-data calibrated box model, J. Hazardous Materials, 8 (1984) 205—221.
17 G.D. Raithby, A critical evaluation of upstream differencing applied to problems involving fluid flow, Comp. Meth. Appl. Mech. Eng., 9 (1976) 75—103.
18 D.L. Book, J.P. Borris and K. Hain, Flux corrected transport III: Minimal-error FCT algorithms, J. Comp. Phys., 20 (1976) 397—431.
19 R.G. Picknett, Dispersion of dense gas puffs released in the atmosphere at ground level, Atmos. Environ., 15 (1981) 509—525.
20 D.J. Hall, E.J. Hollis and H. Ishaq, A wind tunnel model of the Porton dense gas field trials, Warren Springs Laboratory Report L394(AP), Dept. of Industry, Stevenage, Hertfordshire, U.K., 1982, 106 pp.
21 J.S. Puttock, D.R. Blackmore and G.W. Colenbrander, Field experiments on dense gas dispersion, J. Hazardous Materials, 6 (1982) 13—42.
22 R.P. Koopman, R.T. Cederwall, D.L. Ermak, H.C. Goldwire, Jr., W.J. Hogan, J.W. McClure, T.G. McRae, D.L. Morgan, H.C. Rodean and J.H. Shinn, Analysis of Burro series 40 m^3 LNG spill experiments, J. Hazardous Materials, 6 (1982) 43—84.
23 R.N. Meroney and D.E. Neff, Physical modeling of forty cubic meter LNG spills at China Lake, California, in: C. de Wispelaere (Ed.), Air Pollution Modeling and Its Applications, Vol. 1, Plenum, New York, pp. 24—27.
24 G. Andreiev, D.E. Neff and R.N. Meroney, Heat transfer effects during cold dense gas dispersion, Gas Research Institute Report No. GRI 83/0082, Chicago, Illinois, U.S.A., 1983, 241 pp.